Received: 14 July 2020 | Revised: 9 February 2021 | Accepted: 14 February 2021

DOI: 10.1111/gbi.12439

ORIGINAL ARTICLE

gebiology WILEY

Phosphatic scales in vase-shaped microfossil assemblages from Death Valley, Grand Canyon, Tasmania, and Svalbard

Leigh Anne Riedman[1,2] | Susannah M. Porter[2] | Andrew D. Czaja[3]

[1]Department of Earth and Planetary Sciences, Harvard University, Cambridge, MA, USA

[2]Department of Earth Science, University of California at Santa Barbara, Santa Barbara, CA, USA

[3]Department of Geology, University of Cincinnati, Cincinnati, OH, USA

Correspondence
Leigh Anne Riedman, Department of Earth Science, University of California at Santa Barbara, Santa Barbara, CA 93106, USA.
Emails: lariedman@gmail.com, lriedman@ucsb.edu

Funding information
Cushman Foundation for Foraminiferal Research; NASA Astrobiology; Palaeontological Association; University of Cincinnati, Department of Geology; National Science Foundation, Grant/Award Number: EAR-0922305

Abstract

Although biomineralized skeletal elements dominate the Phanerozoic fossil record, they did not become common until ~550–520 Ma when independent acquisitions of biomineralization appeared in multiple lineages of animals and a few protists (single-celled eukaryotes). Evidence of biomineralization preceding the late Ediacaran is spotty aside from the apatitic scale microfossils of the ~811 Ma Fifteenmile Group, northwestern Canada. Here, we describe scale-shaped microfossils from four vase-shaped microfossil (VSM)-bearing units of later Tonian age: the Togari Group of Tasmania, Chuar and Pahrump groups of southwestern United States, and the Roaldtoppen Group of Svalbard. These scale-shaped microfossils consist of thin, ~13 micron-long plates typically surrounded by a 1–3 micron-thick colorless envelope; they are found singly and in heterotypic and monotypic clusters of a few to >20 specimens. Raman spectroscopy and confocal laser scanning microscopy indicate these microfossils are composed of apatite and kerogen, just as is seen in the Fifteenmile Group scale microfossils. Despite compositional similarity, however, these scales are probably not homologous, representing instead, an independent acquisition of apatite mineralization. We propose that these apatite-kerogen scale-shaped microfossils are skeletal elements of a protistan cell. In particular, their consistent co-occurrence with VSMs, and similarities with scales of arcellinid testate amoebae, a group to which the VSMs are thought to belong, suggest the possibility that these microfossils may be test-forming scales of ancient arcellinid testate amoebae. The apparent apatite biomineralization in both these microfossils and the Fifteenmile scales is unexpected given its exceedingly rare use in skeletons of modern protists. This modern absence is attributed to the extravagance of using a limiting nutrient in a structural element, but multiple occurrences of apatite biomineralization in the Tonian suggest that phosphorus was not a limiting nutrient for these organisms, a suggestion consistent with the idea that dissolved seawater phosphate concentrations may have been higher at this time.

KEYWORDS

apatitic scale microfossils, biomineralization, Neoproterozoic, phosphorus, Tonian, vase-shaped microfossil

1 | INTRODUCTION

Mineralized skeletons evolved dozens of times within the eukaryotes and are distributed widely across the tree, occurring in every major clade (Knoll, 2003). It is therefore puzzling that, despite the fact that eukaryotic fossils are found in rocks as old as 1.6 Ga (Javaux, 2007; Lamb et al. 2009; Peng et al., 2009), fossils of skeletal-mineralizing eukaryotes are virtually absent from rocks >550 Ma (Wood, 2018). Several reports suggest evidence of older possible mineralized organisms such as fossils interpreted as algal sheets (Horodyski & Mankiewicz, 1990), as scale-bearing protists (Porter et al., 2003) or protists with homogeneous mineralized tests (Morais et al., 2017), but these reports are not confirmed. The notable exception to this lack of confirmed pre-Ediacaran biomineralizers is the assemblage of scale microfossils known only from the c. 811 Ma Fifteenmile Group of northwestern Canada (Allison, 1981; Allison & Hilgert, 1986; Cohen & Knoll, 2012; Cohen et al., 2011, 2017). First assumed to be siliceous (Allison, 1981; Allison & Hilgert, 1986), recent work has shown the Fifteenmile scale microfossils consist of kerogen and apatite in the form of interwoven fibrous hydroxyapatite crystals (Cohen et al., 2011; Cohen, Strauss, et al., 2017), which is particularly intriguing because today phosphate skeletal mineralization is almost exclusively restricted to animals, occurring commonly in only lingulate brachiopods and vertebrates (Knoll, 2003) and the arcellinid testate amoeba *Cryptodifflugia oviformis* (Hedley et al., 1977) and perhaps in the green algae *Mesostigma viride* (Domozych et al., 1991).

Here, we describe scale-shaped microfossils from four vase-shaped microfossil-bearing units of late Tonian age: the Togari Group of Tasmania, the Chuar and Pahrump groups of the southwest United States, and the Roaldtoppen Group of Svalbard (Figure 1). These new microfossils appear similar to, but are probably not homologous with, the apatitic scale microfossils of the Fifteenmile Group; rather we speculate that these newly reported fossils may represent test-forming scales of a vase-shaped microfossil.

SUMMARY STATEMENT

Here, we report apatite-kerogen scale-like structures from four globally distributed, vase-shaped microfossil-bearing late Tonian units. Raman spectroscopy and confocal laser scanning microscopy confirm a composite apatite and kerogen composition. Although these new microfossils are similar in composition to the c. 811 Ma Fifteenmile Group scales, they are not considered likely to be homologous, but instead, given their association with VSMs and similarity to modern arcellinid scales, are interpreted as possible scale elements of arcellinid testate amoebae.

2 | GEOLOGIC SETTING

In the lower Black River Dolomite of northwestern Tasmania, abundant scale microfossils occur with vase-shaped microfossils (VSMs) in early diagenetic bedded and nodular cherts and gray mudstones that record shallow marine to lagoonal deposition (Figure 1; Tables S1 and S2; Calver, 2011). The Black River Dolomite underlies the Julius River Member, a diamictite of presumed Sturtian age (Calver, 2011; Rooney et al., 2015). Tens of meters above the fossil horizons, the Black River Dolomite hosts a carbon isotopic excursion correlated with the c. 740–732 Ma negative $\delta^{13}C$ anomaly in the Callison Lake Formation of Canada (Calver, 1998; Strauss et al., ,2014, 2015).

In the Chuar Group, scale microfossils occur in chert nodules within carbonates 3.6 meters above the base of the Walcott Member of the Kwagunt Formation, and within VSM-bearing shales in the lower half of the Walcott Member. Deposition of the Kwagunt Formation is interpreted to have occurred in a variably restricted, low-energy marine subtidal to intertidal setting (Dehler et al., 2001, 2012). Deposition of scale-bearing strata of the Walcott Member is constrained to have occurred between 751.0 ± 7.6 and 729.0 ± 0.9 Ma based on Re-Os geochronology of marcasite nodules from the subjacent Awatubi Member and a U-Pb zircon age from a tuff in the uppermost Walcott Member (Rooney et al., 2017).

In the Pahrump Group of Death Valley, California, scale microfossils occur in VSM- bearing silicified carbonates of the "upper cherty member" of the Beck Spring Dolomite (Figure 1). Licari illustrated similar structures from the Beck Spring Dolomite at a locality near Horse Thief Springs in the Kingston Range (Licari, 1978); we examined Licari's samples and additional specimens collected from Alexander Hills ~20 km to the west. The Beck Spring Dolomite is interpreted to record a shallow-water carbonate environment (Harwood & Sumner, 2011). Its age is constrained to 787–732 Ma by detrital zircons in the underlying Horse Thief Springs Formation (Mahon et al., 2014) and a negative $\delta^{13}C$ excursion in the uppermost portion of the unit correlated with the c. 740–732 Ma Callison Lake anomaly (Macdonald et al., 2013; Smith et al., 2015; Strauss et al., 2014).

Finally, scale microfossils occur in silicified VSM-bearing pyritic black shales of the upper Ryssö Formation, Roaldtoppen Group, Nordaustlandet, Svalbard (Figure 1), interpreted to record intertidal to very shallow subtidal marine deposition in a coastal carbonate flat (Knoll & Calder, 1983). The Ryssö Formation, a lateral equivalent of the upper Akademikerbreen Group of Spitsbergen, underlies the Sturtian-equivalent Backaberget Formation and is constrained to be ~810–752 Ma based on a subsidence-age model (Halverson et al., 2018).

3 | METHODS

All specimens were studied in 60 micron-thick petrographic thin sections. Three thin sections of the Beck Spring Dolomite described by Licari (1978; slides C250 (11), C250 (38), C250 (39)) and stored at the Smithsonian Institute, Washington, D.C., were studied with a Nikon Eclipse 80i transmitted light microscope. Sample K1355-5D of the

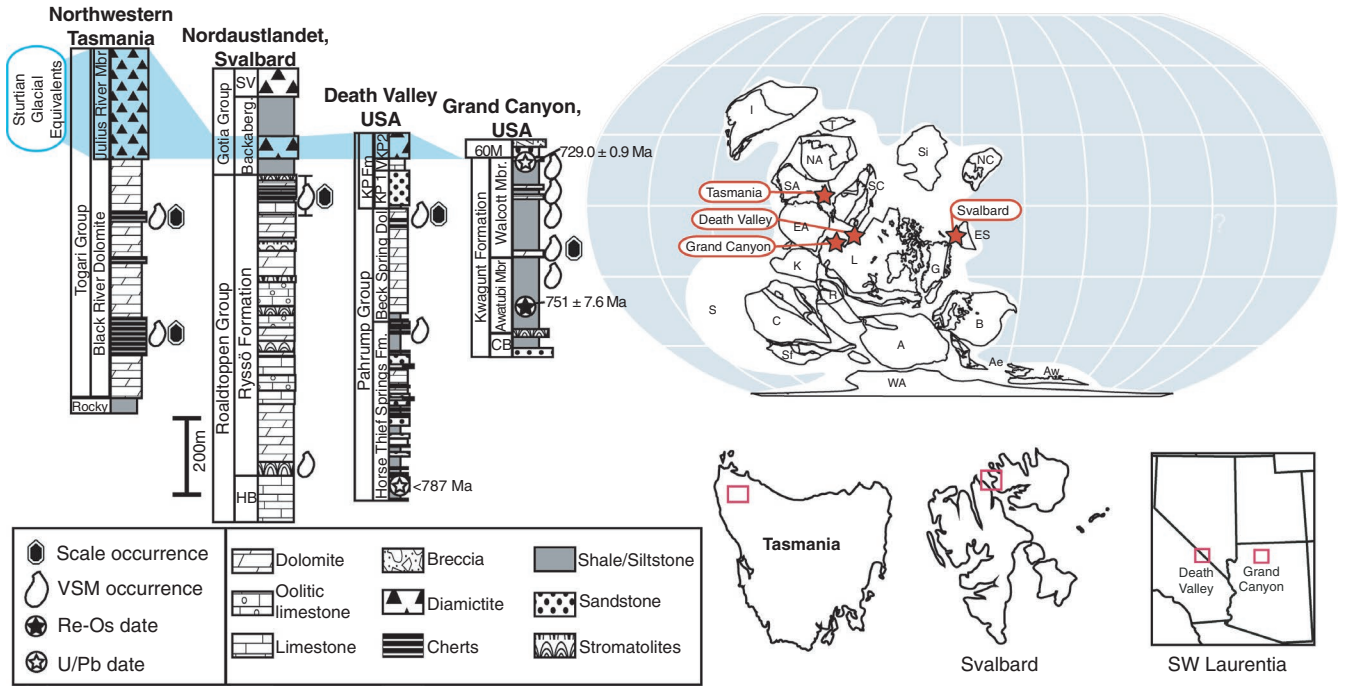

FIGURE 1 Stratigraphic columns, paleogeographic reconstruction, and locality maps. Stratigraphic correlation with VSM placements modified from Riedman et al. (2018). Paleogeographic reconstruction indicating depositional localities ~780 Ma, adapted from Li et al. (2013). Stratigraphic column abbreviations: Rocky = Rocky Cape Group, HB = Hunnberg Fm., Backaberg. = Backaberget Fm. SV = Sveanor Fm., KP = Kingston Peak Fm, KP1, KP2 = Kingston Peak units 1 and 2 (informal), V = Virgin Spring Limestone, CB = Carbon Butte Member, 60 M = Sixtymile Fm. Maps of Tasmania, Svalbard and southwestern United States, red boxes indicate sample localities. References: Tasmania: Calver (1998, 2011); Nordaustlandet: Knoll and Calder (1983); Death Valley: Dehler (2014); Horodyski (1993); Mahon et al. (2014); Smith et al. (2015); Grand Canyon: Dehler et al. (2001), Porter and Knoll (2000); Porter et al. (2003); Rooney et al. (2017), Karlstrom et al. (2018)

Ryssö Formation, collected and first described by Knoll and Calder (1983), is part of the Harvard University Paleobotanical Collections and was studied using a Leitz Orthoplan microscope. Samples AK-10-53-6 and C.shale1-11/16 from the Walcott Member, Kwagunt Formation, Chuar Group are part of Porter's sample collection at University of California at Santa Barbara. These and following samples were studied at UCSB using a Zeiss Axioskop 40 transmitted light microscope. Samples BSF-17-4-02 and BSF-17-4-05, Tas 10-18A, Tas 10-18B, Tas 10-24 and Tas 10-41 are currently stored at UCSB. The focus-stacking software package Helicon Focus was used merge images at several focal depths in Figures 2.3, 2.4, 2.7, 2.9, 2.11, 2.13, 2.14, 2.16 and 3.6.

Confocal laser scanning microscopy (CLSM) was performed on sample Tas 10-18B at the NRI-MCDB microscopy facility at UCSB using an Olympus Fluoview 1000S Spectral Confocal microscope, and on samples Tas 10-18B, BSF-17-4-02A and AK-10-53-6B at University of Cincinnati using an Olympus Fluoview 1200 CLSM running the FV10-ASW software (v. 3.01). CLSM images were acquired by use of 458, 488, and 635 nm laser excitation (<300 μW at the sample), a 60X oil-immersion objective (NA [numerical aperture] = 1.42) with fluorescence-free microscopy immersion oil (Olympus Type-F). Bandpass filters of 480–495 nm, 505–605 nm, and 655–755 nm were used to exclude the incident laser wavelengths of 458, 488, and 635 nm, respectively.

For 3-D animations, 2-D images were exported as TIF files and rendered into 3-D images and animated with the software program Paraview v. 5.0.1 (Kitware Inc.).

Raman spectroscopy was performed on samples Tas 10-18B, AK-10-53-6a, AK-10-53-6b, BSF 17-4-02A, and BSF 17-4-05A at the University of Cincinnati using a Horiba T64000 Raman microscope, a 50X long working distance objective (NA = 0.50), and 457.9 nm excitation from a Coherent FreD 90C Ar+ laser with a spot size of ~1 μm. Laser power was kept to ≤9 mW at the sample and was determined not to have caused sample alteration. Raman spectra had very minor backgrounds, so no baseline subtraction was needed. Two-dimensional Raman maps were created by acquiring spectra in a grid with 1 μm pixel spacing and integrating the spectral intensity from 440–490 cm^{-1}, 950–980 cm^{-1}, and 1275–1425 cm^{-1} for quartz, apatite, and kerogen, respectively.

4 | FOSSIL DESCRIPTIONS

4.1 | Morphology

The scale microfossils were all observed in thin sections of cherts and shales, and specimens ($N > 300$) are found both singly and in monotypic (Figure 2.18, Figure S7) and heterotypic (Figure 2.16,

FIGURE 2 Solitary and clustered scale microfossils. Morphotypes: shield (1–3, 5, 7, 17 *in part*), square (6, 16 *in part*), surfboard (4, 8, 14), pennate (9, 11, 13, 18), oval (10, 12), heterotypic clusters (16, 17), monotypic cluster (18). Inset line drawing of 18 illustrates left-most scale in which organic contents of inner plate no longer meet plate boundary, which is denoted by dotted line. See Figure S7 for transmitted light animation of 18. VSMs and oval scale (arrow;15). From Beck Spring Formation (1, 9, 10, 12), Black River Dolomite (2, 4, 8, 11, 13–16, 18), Kwagunt Formation (3, 6, 7, 17), Ryssö Formation (5). Scale bar is 25μm for 1–14, 140 μm for 15, and 35 μm for 16–18

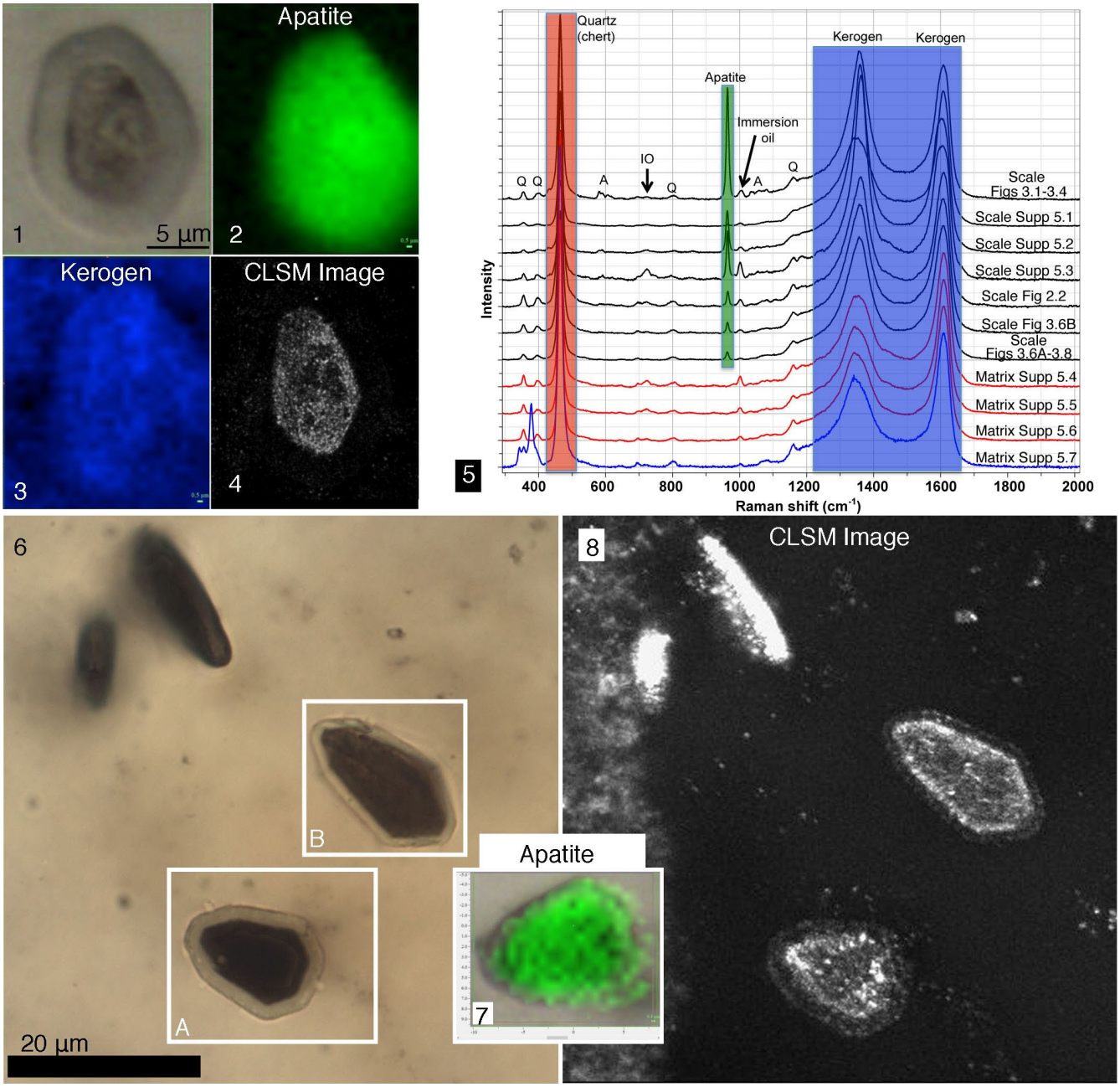

FIGURE 3 Raman images, Raman spectra, and confocal laser scanning microscopy (CLSM) images of scale microfossils. 1–4) same specimen viewed in 1) transmitted light microscopy, 2) Raman image of apatite abundance derived from apatite region of spectrum, 3) Raman image of kerogen abundance derived from kerogen region of spectrum, 4) CLSM image, likely indicative of kerogenous composition, particularly of inner portion of scale. 5) Raman spectra of seven scale microfossils (Figures 2 and 3; Figure S5) and four matrix regions, illustrating apatite is found only in scales, not dispersed throughout the matrix. 6, 8) Transmitted and CLSM images of scale cluster. As above, fluorescence in CLSM is likely indicative of kerogen signal. Inset boxes in 6 labeled A and B indicate these scales were analyzed to produce spectra in 3.5. 7) Raman imagery derived from apatite signal for scale in 6A. All specimens from Black River Dolomite, sample Tas 10-18B-LAR. Scale in 1 applies to 1–4, and scale in 6 applies to 6–8. See Figure S2a,b for animations of specimens in 3.1–3.4 and 3.6–3.8, respectively

2.17) clusters of a few to more than 20 specimens. They consist of a typically brown to black, flat plate that is 1.0 to 4.0 µm thick (mean = 2.1 µm, $N = 14$), 2.0–16.3 µm wide (mean = 6.2 µm, $N = 141$), and 6.3–27.6 µm long (mean = 13.3 µm, $N = 133$) that in the majority of specimens is surrounded by a lighter colored-to-colorless envelope (Figures 2 and 3).

The darker internal plate varies from nearly opaque and homogenous (e.g., Figures 2.4, 2.8, 2.18 and 3.6a,b) to mottled (Figure 2.1, 2.3, 2.7, 2.9, 2.12), to translucent (e.g., Figure 2.2, 2.14), sometimes with only hints of a darker color visible at the boundary with the outer layer (Figure 2.6, 2.16). In some specimens, the darker material is clotted in appearance and has pulled away from the plate's

boundary with the envelope, leaving a translucent area between them, but maintaining the original plate shape (Figure 2.18, arrow indicates pennate plate shape is retained despite degradation of organic material, see also inset line drawing). The lighter colored-to-colorless envelope fully encapsulates the darker internal plate; this is apparent, as is the plate's flat nature, when specimens are viewed edge-on, when focusing through the depth of the specimen in transmitted light microscopy (Figure S1), and in three-dimensional confocal laser scanning microscopy reconstructions (Figure 3.8; Figure S2a,b). The envelope ranges in thickness from 0.9 to 8.7 μm (mean=2.6 μm, N = 128). In some specimens, concentric rings are visible within the envelope (e.g., Figure 2.1, 2.6, 2.12). No correlation has been found between the thickness of the envelope and scale morphotype, size of internal plate, locality, or sample (Figure S3).

No scale microfossils have been found bent or distorted, but the envelope occasionally (N = 11) displays abrasion and breakage (Figure 2.1, 2.11, 2.13); rarely, this breakage also affects the plate (Figure 2.4, 2.13). Some specimens exhibit blunt-edged, colorless crystals that radiate in all directions from the exterior of the fossil (Figure 2.9, 2.12; Figure S4).

Several morphotypes have been recognized, composing similar but not identical assemblages across the four units described here (Figures 2 and 4; Tables S1 and S2). These include oval forms (N = 38) that average 11.0 by 5.6 μm in plate length (L_{plate}) and plate width (W_{plate}), respectively, and 16.3 by 10.7 μm, respectively, in overall (plate + envelope) length ($L_{overall}$) and overall width ($W_{overall}$); pennate forms, with pointed to flattened ends (N = 39; L_{plate} = 18.6 μm, W_{plate} = 5.7 μm; $L_{overall}$ = 24.1 μm, $W_{overall}$ = 9.9 μm); "surfboard" morphotypes, elongate with one rounded or pointed end and one flattened end (N = 20; L_{plate} = 13.7 μm, W_{plate} = 4.8 μm; $L_{overall}$ = 18.6 μm, $W_{overall}$ = 8.7 μm); shield morphotypes, with 5 to 7 sides (N = 48; L_{plate} = 11.1μm, W_{plate} = 7.8 μm; $L_{overall}$ = 15.6 μm, $W_{overall}$ = 12.4 μm) and square morphotypes (N = 5, L_{plate} W_{plate} = 8.2 μm; $L_{overall}$ and $W_{overall}$ = 12.8 μm). Particular attention was paid to avoiding conflating elongate or pennate morphotypes with specimens of other morphotypes viewed in an edge-on orientation. This was mitigated by viewing specimens throughout their depth within the thin section (e.g., Figures S1, S4 and S7).

4.2 | Composition

Raman spectroscopy was used to determine scale microfossil compositions. Raman spectra collected from twenty-four microfossils (Figure 3.5; Figures S5, S6 and S9) and Raman images of sixteen (e.g., Figure 3.2, 3.3, 3.7; Figures S6 and S9) indicate they are composed of apatite (major peak at 965 cm^{-1}) and varying amounts of kerogen (major bands between 1,200 and 1,700 cm^{-1}). Peaks

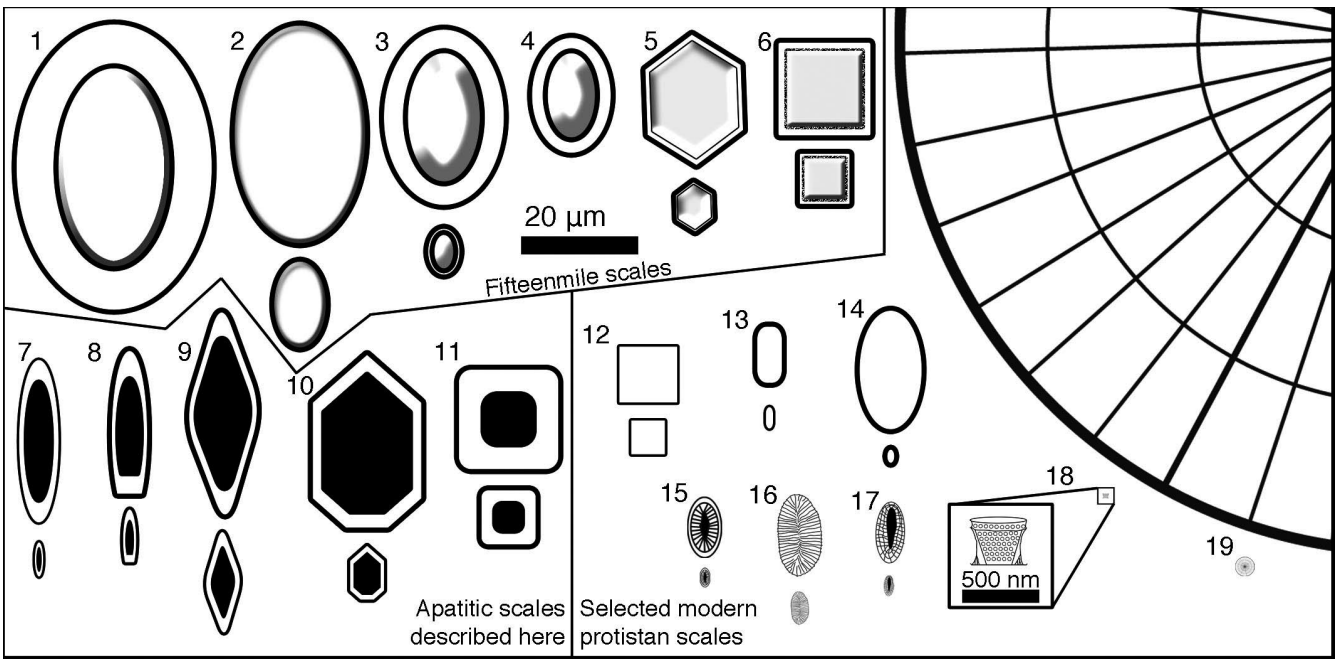

FIGURE 4 Size comparison of apatitic scale microfossils and selected modern scale-bearing protists. Illustrations of largest and smallest specimens recorded for taxa; where only one individual of a taxon is illustrated the size difference is negligible among measured specimens. 1–6) apatitic scale microfossils of the Fifteenmile Group (Allison & Hilgert, 1986; Cohen & Knoll, 2012); 7–11) apatitic scale microfossils from units described here; 12–18) Modern scale-bearing protists. 1) *Bicorniculum brochum*; 2) *Archeoxybaphon* spp. 3) *Paleomegasquama arctoa*; 4) *Petasisquama petasus*; 5) *Hexacatillus allmonii*; 6) *Paleoscutula* spp.; 7) oval morphotype; 8) surfboard morphotype; 9) pennate morphotype; 10) shield morphotype; 11) square morphotype; 12) siliceous scale of *Quadrulella* sp. (Arcellinida; Kosakyan et al., 2016); 13) siliceous scale of *Pomoriella valkanovi* (Arcellinida; Golemansky & Todorov, 2004); 14) euglypid (Rhizaria) scale (Ogden & Hedley, 1980); 15) coccolithophore coccolith (Young et al., 2003); 16) centrohelid heliozoan scale (Zlatogursky, 2016); 17) Synurophyte scale (Preisig, 1994); 18) *Mesostigma viride* (Domozych et al., 1991) basket scale; 19) Diatom frustule—note upper size range frustule above "19" label (Snoeijs et al., 2002). Scale bar below 4 applies to all except zoom-in box of 18

representing kerogen and quartz (from the chert matrix) are present in all spectra of the scales and matrix; peaks from immersion oil (from thin section surface) are present in some, but there is no evidence of calcite or other carbonates in any spectra. Raman spectra and images were collected using a confocal aperture, so the detected signals are spatially resolved in the X, Y, and Z axes, insuring that spectra collected from the scales are indeed reflecting the composition of the scale and not over- or underlying matrix. Raman imaging of scales (Figure 3.2, 3.3, 3.7; Figures S6 and S9) and spectra collected in four points in the matrix (Figure 3.5; Figures S5 and S9) illustrate the spatial distribution of apatite and kerogen, demonstrating that apatite is found only within the scales and blunt-edged, radiating crystals and is not otherwise found in the matrix, and that although kerogen is present within both the matrix and the scales, it is typically in greater abundance within the scales than the matrix.

Two- and three-dimensional images created by confocal laser scanning microscopy (CLSM), performed on twenty-one scales and surrounding matrix, are also consistent with the presence of apatite and kerogen in the scales, showing higher abundances in the inner plates than in the envelopes (Figure 3.4, 3.8; Figures S2 and S6). Although CLSM imagery is not specifically diagnostic of composition, both apatite and kerogen are known to fluoresce in this range (between 505 and 605 nm; Cohen et al., 2011). Thus, CLSM and Raman data both suggest these scale microfossils are composed of apatite, with a relatively more kerogen-rich inner plate and more kerogen-poor envelope.

5 | INTERPRETATION OF APATITE-KEROGEN MINERALIZATION

We hypothesize that the plates of these microfossils are biological structures similar to scales of modern single-celled eukaryotes (protists). This is based on their organic nature, their consistent shapes and sizes within and across assemblages, and on the fact that their sizes, size ranges, and clustering habits are consistent with those known from modern protistan scales (Figure 4). Although some shapes could be explained by unusual apatite crystal habits (e.g., the flat hexagon; Figure 2.7), the unusual shapes and rounded edges (e.g., oval, surfboard, pennate) of others are difficult to explain in this way. Furthermore, occurrence of these same morphotypes in rocks of the same age from across the globe—all in association with vase-shaped microfossils—supports the idea that they are biological, that is, taxa with a unique stratigraphic range, rather than crystals. Finally, evidence of tearing in some specimens (Figure 2.4, 2.13) suggests the plate began as an organic template that was later mineralized, as opposed to an abiotic mineral that incorporated ambient organic material during growth. Such organic templating is common in modern biomineralized structures, creating composites that are both rigid but yielding enough to resist breakage (Ehrlich, 2010).

Our observations suggest three stages of apatite mineralization in these microfossils: (1) the apatite-kerogen plate, (2) the apatite-kerogen envelope, found in nearly all specimens, and (3) the needle-like apatite crystals, found in some specimens (e.g., Figure 2.9, 2.12). Several observations indicate the plate (stage 1) was mineralized in life. First, specimens that exhibit degraded organic cores nonetheless show a regular, consistent shape (e.g., oval, surfboard) along the boundary between the plate and envelope (e.g., arrow in Figure 2.18), rather than a boundary tracing the irregular outline of degraded organic material. This indicates that apatite mineralization occurred prior to organic matter degradation and must have been either biogenic or emplaced very shortly after death or shedding. The latter possibility that secondary mineralization of the plates could have proceeded so swiftly and evenly after death in every scale specimen in each of these widely separated basins seems unlikely, especially given abundant evidence for degradation that occurs in organic fossils that are known to be secondarily phosphatized (e.g., Briggs, 2003; Briggs & Wilby, 1996; Creveling et al., 2014; Xiao & Knoll, 1999). Additionally, if the plates had been originally organic and unmineralized, we might reasonably expect to find unmineralized or partially mineralized plate specimens as well as fragmentary organic plates in the assemblages. In fact, whole or fragmentary unmineralized organic plates have never been found in any of these assemblages despite a reasonable expectation of organic preservation given the occurrence of organic-walled microfossils such as likely cyanobacterial filaments (*Siphonophycus*) and smooth-walled acritarchs (*Leiosphaeridia* spp.).

Whether the second observed stage of apatite mineralization—the apatite-kerogen envelope—was biological is more difficult to determine. Similar, concentrically biomineralized structures are known from a variety of modern organisms (e.g., pearls and otoliths), but the possibility that the envelope resulted from abiotic coating cannot be discounted. Although other organic structures in the same samples (e.g., acritarchs and filaments) do not show any evidence of apatite coating, possible coatings do occur on small particles (Figure S8a,b). These small particles could be additional examples of biogenic apatitic fossils, or perhaps a secondary, abiotic coating preferentially nucleated on particles and plates instead of acritarchs due to compositional differences (e.g., Donoghue et al., 2006). Further, the discovery (although of only one instance) of two scales apparently fused at the envelope, might argue for a diagenetic origin of the envelope (Figure S8c). However, if the envelopes were secondary, we would also expect to find a varied collection of nuclei including fragmentary plates and rip-up clasts rather than the consistent shapes, sizes, and compositions seen across these four units. A small number of scale specimens lack envelopes (Figure 2.2, 2.14); these could be rare morphotypes that lacked a biogenic envelope, or they could simply represent the apatite-kerogen scale as it looked in life before coating.

Finally, the third stage of apatite mineralization, precipitation of needle-like apatite crystals that radiate from many specimens, seen especially in scales from Beck Spring Dolomite and Black River Dolomite (Figure 2.9, 2.12; Figures S4 and S6), is inconsistent with a biological origin and instead is interpreted to have occurred after death or shedding.

In summary, we interpret these structures to be a composite of both biogenic and non-biogenic apatite mineralization. The internal, kerogen-rich plates (and perhaps, surrounding envelopes) were mineralized during life, and in some cases, these microfossils were further coated with abiotic apatite needles. Because these needles radiate in all directions, having grown unencumbered; and because (with one exception, Figure S8c) the envelopes are never observed growing together, even in clusters where they are <1 μm apart; and because some specimens have broken (Figure 2.13) or abraded envelopes (Figure 2.1, 2.8), we hypothesize that all stages of apatite mineralization likely occurred at the sediment–water interface or in the water column, rather than within pore spaces of the sediment after burial. This suggests that within these four widely distributed basins, seawater phosphate concentrations were high enough to support both apparent biogenic and abiotic apatite precipitation (e.g., Cohen, Strauss, et al., 2017), consistent with predictions from weathering models (Goddéris et al., 2017; Hartmann et al., 2014) and other P proxies (Lenton & Daines, 2018; Reinhard et al., 2017).

5.1 | Comparison with fifteenmile scale microfossils

Some morphotypes of the apatite-kerogen scale microfossils reported here broadly resemble certain taxa of apatitic scales described from the Fifteenmile Group (Allison & Hilgert, 1986; Cohen & Knoll, 2012; Cohen et al., 2011; Cohen, Strauss, et al., 2017) and microfossils recently reported from the Visingsö Group of Sweden (Moczydłowska et al., 2017). Although elaborate, perforate and ornamented Fifteenmile scales are the ones that spring most readily to mind, more than half of the genera described by Allison and Hilgert (1986) and Cohen and Knoll (2012) have solid, imperforate plates with minor or no spines or further ornament, similar to the scales reported here.

The oval morphotype described here is similar to the imperforate oval forms *Archeoxybaphon* (Figure 4.2), *Paleomegasquama* (Figure 4.3), *Petasisquama* (Figure 4.4), and *Bicorniculum* (Figure 4.1) of the Fifteenmile assemblage (Allison & Hilgert, 1986; see also Moczydłowska et al., 2017), although the last of these is significantly larger in size (44–52 μm in length), and, along with *Paleomegasquama* has a two-plate construction. (Thus far, no two-plate forms have been identified in the present materials.) Additionally, the shield morphotype (Figures 2.1–2.3, 2.5, 2.7, 2.17 and 4.10) is similar in shape and size to the imperforate hexagonal Fifteenmile scale *Hexacatillus allmonii* (Cohen & Knoll, 2012; Figure 4.5), and the square morphotype (Figures 2.6, 2.16, 4.11) is similar in both shape and size to the Fifteenmile *Paleoscutula* (Cohen & Knoll, 2012; Figure 4.6).

These assemblages differ, however, in several ways: the pennate (Figures 2.9, 2.11, 2.13, 2.18 and 4.9) and surfboard (Figures 2.4, 2.8, 2.14 and 4.8) morphotypes common in the four assemblages described here have not been reported from the Fifteenmile Group, and the many perforate and ornamented forms found in the Fifteenmile assemblage have not been found in our materials (nor reported from the Visingsö Group (Moczydłowska et al., 2017)). Additionally, the apatitic envelope seen in the scales described here is absent from scale microfossils of the Fifteenmile Group. Thus, despite compositional and broad-brush morphological similarities between certain taxa of the Fifteenmile scale assemblage and the new apatitic-kerogen scales described here, these two groups are not considered to be homologous. Rather, these groups appear to represent independent acquisitions of apatite biomineralization during the middle to late Tonian Period.

5.2 | Biological affinities

The character of producing cell-covering scales is widely convergent, having been gained and lost repeatedly in separate lineages (e.g., Howe et al., 2011; Kristiansen & Škaloud, 2017; Zlatogursky, 2016). Although scales of modern protists are widely variable—occurring as external or internal structures, ranging widely in shape and size (e.g., 100s nm to 100s μm; Figure 4), and of variable composition (commonly organic, siliceous, calcareous)—there are no clear homologs among modern groups, in part because protistan use of apatite is exceedingly rare or non-existent (Knoll & Kotrc, 2015; Raven & Knoll, 2010). Further, the occurrence of monotypic or heterotypic microfossil scale clusters cannot inform biological placement because the capacity for an individual cell to produce several distinct scale morphotypes at any given time is a commonly held convergent trait across modern species, seen for example, in coccolithophores (Young et al., 2005), amoebozoan and rhizarian testate amoebae (Ogden & Hedley, 1980), and chrysophytes (Kristiansen & Škaloud, 2017).

Nonetheless, there are some intriguing similarities with a few modern groups. Siliceous scales produced by some centrohelid heliozoans are similar in size and shape to the scale microfossils described here, including the sort of three-dimensional sculpture seen in the shield specimen in Figure 2.3 (Figure 4.16; e.g., Gast, 2012; Zlatogursky, 2013, 2016; see also Cohen et al., 2011 who made a similar comparison for Fifteenmile Group apatitic scales), but use of apatite has not been reported from this group. The scale microfossils described here are also similar in size and shape (if not composition) to some scales produced by members of the Amoebozoa and Rhizaria (Ogden & Hedley, 1980; Figure 4.12–4.14). In fact (and discussed in detail below), vase-shaped microfossils, a group allied with the arcellinid Amoebozoa (Porter & Knoll, 2000; Porter & Riedman, 2019), occur in all of the samples as the scales presented here (Knoll & Calder, 1983; Porter & Knoll, 2000; Horodyski, 1993; Porter et al., 2003; Dehler, 2014; Riedman et al., 2018; Figure 2.15) as well as in the Visingsö Group of Sweden (Martí Mus & Moczydłowska, 2000; Moczydłowska et al., 2017).

Of course, an additional possibility, given the widespread convergent acquisition of scales among eukaryotes, is that these microfossils could represent yet another independent acquisition of body-covering scale elements in a clade that is now extinct.

5.3 | Association with vase-shaped microfossils

The apatitic scale microfossils reported here are all found to co-occur with vase-shaped microfossils (VSMs). Not all VSM-bearing units, however, have been found to host these scale microfossils; for example, our study of VSM samples from dolomite nodules in the upper Chuar Group (Porter & Knoll, 2000; Porter et al. 2003) and from the Callison Lake Formation (Riedman et al., 2018; see also Strauss et al., 2014 and Cohen et al., 2017 for VSMs of Callison Lake) have revealed no apatitic scale-like structures. Further, non-VSM-bearing units (e.g., Svanbergfjellet, Myrtle Springs, Skillogalee, and Doushantuo formations) studied by the authors have not been found to host these scale forms, which is supportive of their limited stratigraphic range. Certainly, the absence of scales from non-VSM-bearing units, and the occurrence of scales where we do see VSMs, does not prove that the scales must be biologically associated with the VSMs, but these observations are consistent with that scenario.

The co-occurrence of VSMs and the scale microfossils reported here may be ecological, reflecting a common reliance on a temporally and locally constrained resource and a shared habitat preferences (e.g., shallow marine environments); or it may be preservational, reflecting the happenstance of a shared taphonomic window (albeit a wide one, Cohen, Irvine, et al., 2017; Riedman et al., 2018). Alternatively, this co-occurrence could reflect a biological signal indicating that these apatitic scale microfossils derive from individuals within the VSM group (e.g., the VSM *Melicerion poikilon* has been suggested to have borne scales, Porter & Knoll, 2000; Porter et al., 2003). As mentioned above, VSMs have been robustly allied with the Arcellinida, a major group of test (shell) forming single-celled eukaryotes (Porter & Riedman, 2019). Intriguingly, although no known modern arcellinid forms organic scales that are coated and imbued with apatite, some are known to produce tests from organic or mineralized scales, some taxa coat their scales or exogenous particles with resistant organic material or with biosilica (Anderson, 1987), and one taxon (*Cryptodifflugia*) has been reported to coat the inside of its organic test with calcium phosphate (Hedley et al., 1977). Additionally, although some scale-forming and agglutinating taxa embed test-forming elements into a robust organic matrix, which might be expected to retain a recognizable test shape through fossilization, others instead construct tests by cementing scales or particles with a more labile organic cement, which is suggested to decay and collapse upon death (Mitchell et al., 2008 and references therein), a finding consistent with occurrences reported here of disarticulated individual occurrences and disorganized clusters of apatite-kerogen scales structures. Thus altogether, these observations from modern testate amoebae suggest that these individual characters occur within the clade and that their combination in a single species would not be unexpected.

6 | CONCLUSIONS

We propose that the apatite-kerogen scale-shaped microfossils described here are skeletal elements of a protistan cell. Their co-occurrence with vase-shaped microfossils (VSMs) across four globally distributed Tonian units, as well as observed similarities with scales of modern arcellinid testate amoebae (closely allied with the VSMs) suggest the possibility that the microfossils described here may be test-forming scales of ancient arcellinid testate amoebae. Although no modern arcellinid is known to produce structures identical to those described here, the traits needed to make and use these structures are within the arcellinid toolkit.

The apparent biomineralization with apatite seen in these fossils is unexpected given its exceedingly rare use in skeletons of modern protists, an absence attributed to the extravagance of using a limiting nutrient as a structural element. That the only other Tonian occurrence of biomineralized skeletons, the Fifteenmile Group scale microfossils, are also composed of apatite and kerogen, suggests that phosphorus was not a limiting nutrient for these organisms, consistent with the idea that dissolved phosphate concentrations in seawater may have been higher at this time.

Biologically directed mineral formation, biomineralization, did not become common until the latest Ediacaran and early Cambrian periods (~550–520 Ma) when mineralized skeletons evolved numerous times independently in animals and a few protistan groups. A deeper origin of biomineralization, however, is seen in protists of the Tonian Period, and although much is left to decipher regarding the environmental and/or ecological drivers of Tonian protistan biomineralization and biomineral choice, and why this trait did not become more widespread (or more widely preserved) throughout the rest of the Neoproterozoic, the fact that now several occurrences of biomineralized protists have been reported suggests some of those answers may yet be found.

ACKNOWLEDGMENTS

Authors thank three anonymous reviewers for their insightful, helpful, and kind comments. We also thank C. Calver for guidance in the field, Galen Halverson, Chris Junium, Andrew Gangidine, and Jeff Havig for sampling assistance; Galen Halverson, Nicholas Tosca, and John Moore for manuscript feedback; and Stan Awramik for assistance with Preston Cloud's locality notes. Financial support by National Science Foundation: grant EAR-0922305 and Palaeontological Association research grant to S.M.P; NASA Astrobiology Fellowship and Cushman Foundation's Loeblich and Tappan Research award to L.A.R.; and University of Cincinnati, Department of Geology Travel Funding to A.D.C. Thanks also to Ben Lopez and the NRI-MCDB Microscopy Facility at UCSB funded through NIH grant 1 S10 OD010610-01A1, Andrew Knoll for access to Ryssö materials, and Jonathan Wingerath and the Smithsonian Institute for access to microscope facilities and holotype materials reposited by G. Licari, and B.R. and T.R. for technical assistance.

CONFLICT OF INTEREST

The authors declare no competing interests.

AUTHOR CONTRIBUTIONS

LAR and SMP performed transmitted light microscopy, SMP and ADC performed CLSM analyses, and ADC performed Raman

analyses. LAR compiled measurement data. LAR and SMP wrote the manuscript. ADC contributed to the manuscript.

DATA AVAILABILITY STATEMENT

The data that support the findings of this study are available in supplementary tables and from the corresponding author upon reasonable request. Thin sections of original material may be made available to study by contacting the authors.

ORCID

Leigh Anne Riedman https://orcid.org/0000-0002-0959-1674
Susannah M. Porter https://orcid.org/0000-0002-4707-9428
Andrew D. Czaja https://orcid.org/0000-0002-2450-0734

REFERENCES

Allison, C. W. (1981). Siliceous microfossils from the lower Cambrian of Northwest Canada: Possible source for biogenic chert. *Science*, *211*, 53–55. https://doi.org/10.1126/science.211.4477.53

Allison, C. W., & Hilgert, J. W. (1986). Scale microfossils from the early Cambrian of northwest Canada. *Journal of Paleontology*, *60*, 973–1015. https://doi.org/10.1017/S0022336000022538

Anderson, O. R. (1987). Fine structure of a silica-biomineralizing testate amoeba, *Netzelia tuberculata*. *Journal of Protozoology*, *34*(3), 302–309.

Briggs, D. E. G. (2003). The role of decay and mineralization in the preservation of soft-bodied fossils. *Annual Review of Earth and Planetary Sciences*, *31*, 275–301.

Briggs, D. E. G., & Wilby, P. R. (1996). The role of the calcium carbonate-calcium phosphate switch in the mineralization of soft-bodied fossils. *Journal of the Geological Society, London*, *153*, 665–668. https://doi.org/10.1144/gsjgs.153.5.0665

Calver, C. R. (1998). Isotope stratigraphy of the Neoproterozoic Togari Group, Tasmania. *Australian Journal of Earth Sciences*, *45*, 865–874. https://doi.org/10.1080/08120099808728441

Calver, C. R. (2011). Neoproterozoic glacial deposits of Tasmania. In E. Arnaud, G. P. Halverson, & G. Shields-Zhou (Eds.), *Geological record of neoproterozoic glaciations* (Vol. *36*, 649–658). Geological Society of London, Memoirs.

Cohen, P. A., Irvine, S. W., & Strauss, J. V. (2017). Vase-shaped microfossils from the Tonian Callison Lake Formation of Yukon, Canada: Taxonomy, taphonomy and stratigraphic palaeobiology. *Palaeontology*, *60*, 683–701. https://doi.org/10.1111/pala.12315

Cohen, P. A., & Knoll, A. H. (2012). Scale microfossils from the mid-neoproterozoic fifteenmile group, Yukon Territory. *Journal of Paleontology*, *86*, 775–800. https://doi.org/10.1666/11-138.1

Cohen, P. A., Schopf, J. W., Butterfield, N. J., Kudryavtsev, A. B., & Macdonald, F. A. (2011). Phosphate biomineralization in mid-Neoproterozoic protists. *Geology*, *39*, 539–542. https://doi.org/10.1130/G31833.1

Cohen, P. A., Strauss, J. V., Rooney, A. D., Sharma, M., & Tosca, N. (2017). Controlled hydroxyapatite biomineralization in a ~810 million-year-old unicellular eukaryote. *Science Advances*, *3*, e1700095.

Creveling, J. R., Knoll, A. H., & Johnston, D. T. (2014). Taphonomy of Cambrian phosphatic small shelly fossils. *Palaios*, *29*, 295–308. https://doi.org/10.2110/palo.2014.002

Dehler, C. M. (2014). Advances in Neoproterozoic biostratigraphy spark new correlations and insight in evolution of life. *Geology*, *42*, 731–732. https://doi.org/10.1130/focus0812014.1

Dehler, C. M., Elrick, M., Karlstrom, K. E., Smith, G. A., Crossey, L. J., & Timmons, J. M. (2001). Neoproterozoic Chuar Group (~800–742 Ma), Grand Canyon: A record of cyclic marine deposition during global cooling and supercontinent rifting. *Sedimentary Geology*, *141–142*, 465–499. https://doi.org/10.1016/S0037-0738(01)00087-2

Dehler, C. M., Porter, S. M., & Timmons, J. M. (2012). The Neoproterozoic Earth system revealed from the Chuar Group of Grand Canyon. *Geological Society of America Special Papers*, *489*, 49–72.

Domozych, D. S., Wells, B., & Shaw, P. J. (1991). Basket scales of the green alga, Mesostigma viride: Chemistry and ultrastructure. *Journal of Cell Science*, *100*, 397–407.

Donoghue, P. C. J., Kouchinsky, A., Waloszek, D., Bengtson, S., Dong, X.-P., Val'kov, A. K., Cunningham, J. A., & Repetski, J. E. (2006). Fossilized embryos are widespread but the record is temporally and taxonomically biased. *Evolution and Development*, *8*, 232–238. https://doi.org/10.1111/j.1525-142X.2006.00093.x

Ehrlich, H. (2010). Chitin and collagen as universal and alternative templates in biomineralization. *International Geology Review*, *52*, 661–699. https://doi.org/10.1080/00206811003679521

Gast, R. J. (2012). Centrohelida and other heliozoan-like protists. In J. M. Archibald, A. G. B. Simpson, & C. H. Slamovits (Eds.), *Handbook of the protists* (2nd ed, pp. 955–971). Springer International Publishers.

Goddéris, Y., Le Hir, G., Macouin, M., Donnadieu, Y., Hubert-Théou, L., Dera, G., Aretz, M., Fluteau, F., Li, Z. X., & Halverson, G. P. (2017). Paleogeographic forcing of the strontium isotopic cycle in the Neoproterozoic. *Gondwana Research*, *42*, 151–162. https://doi.org/10.1016/j.gr.2016.09.013

Golemansky, V., & Todorov, M. (2004). Shell morphology, biometry and distribution of some marine interstitial testate amoebae (Sarcodina: Rhizopoda). *Acta Protozoologica*, *43*, 147–162.

Halverson, G. P., Porter, S. M., & Gibson, T. M. (2018). Dating the late Proterozoic stratigraphic record. *Emerging Topics in Life Sciences*, *2*, 137–147. https://doi.org/10.1042/ETLS20170167

Hartmann, J., Moosdorf, N., Lauerwald, R., Hinderer, M., & West, A. J. (2014). Global chemical weathering and associated P-release- The role of lithology, temperature and soil properties. *Chemical Geology*, *363*, 145–163. https://doi.org/10.1016/j.chemgeo.2013.10.025

Harwood, C. L., & Sumner, D. Y. (2011). Microbialites of the neoproterozoic beck spring dolomite, Southern California. *Sedimentology*, *58*, 1648–1673. https://doi.org/10.1111/j.1365-3091.2011.01228.x

Hedley, R. H., Ogden, C. G., & Mordan, N. J. (1977). Biology and fine structure of *Cryptodifflugia oviformis* (Rhizopodea: Protozoa). *Bulletin of the British Museum of Natural History*, *30*, 311–328.

Horodyski, R. J. (1993). Paleontology of Proterozoic shales and mudstones: Examples from the Belt Supergroup, Chuar Group and Pahrump Group, western USA. *Precambrian Research*, *61*, 241–278. https://doi.org/10.1016/0301-9268(93)90116-J

Horodyski, R. J., & Mankiewicz, C. (1990). Possible late Proterozoic skeletal algae from the Pahrump Group, Kingston Range, southeastern California. *American Journal of Science*, *290-A*, 149–169.

Howe, A. T., Bass, D., Scoble, J. M., Lewis, R., Vickerman, K., Arndt, H., & Cavalier-Smith, T. (2011). Novel cultured protists identify deep-branching environmental DNA clades of Cercozoa: New genera *Tremula*, *Micrometopion*, *Minimassisteria*, *Nudifila*, *Peregrinia*. *Protist*, *162*, 332–371. https://doi.org/10.1016/j.protis.2010.10.002

Javaux, E. J. (2007). The early eukaryotic fossil record. In G. Jékely (Ed.), *Eukaryotic membranes and cytoskeletons: Origins and evolution* (pp. 1–19). Landes Bioscience and Springer Science + Business Media.

Karlstrom, K., Hagadorn, J., Gehrels, G., Matthews, W., Schmitz, M., Madronich, L., Mulder, J., Pecha, M., Giesler, D., & Crossey, L. (2018). Cambrian Sauk transgression in the Grand Canyon region redefined by detrital zircons. *Nature Geoscience*, *11*, 438–443. https://doi.org/10.1038/s41561-018-0131-7

Knoll, A. H. (2003). Biomineralization and evolutionary history. *Reviews in Mineralogy and Geochemistry*, *54*, 329–356. https://doi.org/10.2113/0540329

Knoll, A. H., & Calder, S. (1983). Microbiotas of the late Precambrian Ryssö Formation, Nordaustlandet, Svalbard. *Palaeontology*, *26*, 467–496.

Knoll, A. H., & Kotrc, B. (2015). Protistan skeletons: A geologic history of evolution and constraint. In C. Hamm (Ed.), *Evolution of lightweight structures biologically inspired systems* (Vol. *6*, pp. 1–16). Springer.

Kosakyan, A., Lahr, D. J. G., Mulot, M., Meisterfeld, R., Mitchell, E. A. D., & Lara, E. (2016). Phylogenetic reconstruction based on COI reshuffles the taxonomy of hyalosphenid shelled (testate) amoebae and reveals the convoluted evolution of shell plate shapes. *Cladistics*, *36*, 606–623.

Kristiansen, J., & Škaloud, P. (2017). Chrysophyta. In J. M. Archibald, A. G. B. Simpson, & C. H. Slamovits (Eds.), *Handbook of the protists* (2nd ed, pp. 331–366). Springer International Publishers.

Lamb, D. M., Awramik, S. M., Chapman, D. J., & Zhu, S. (2009). Evidence for eukaryotic diversification in the ~1800 million-year-old Changzhougou Formation, North China. *Precambrian Research*, *173*, 93–104. https://doi.org/10.1016/j.precamres.2009.05.005

Lenton, T. M., & Daines, S. J. (2018). The effects of marine eukaryote evolution on phosphorus, carbon and oxygen cycling across the Proterozoic-Phanerozoic transition. *Emerging Topics in Life Sciences*, *2*, 267–278. https://doi.org/10.1042/ETLS20170156

Li, Z.-X., Evans, D. A. D., & Halverson, G. P. (2013). Neoproterozoic glaciation in a revised global palaeogeography from the breakup of Rodinia to assembly of Gondwanaland. *Sedimentary Geology*, *294*, 219–232.

Licari, G. R. (1978). Biogeology of the late pre-phanerozoic beck spring dolomite of eastern California. *Journal of Paleontology*, *52*, 767–792.

Macdonald, F. A., Prave, A. R., Petterson, R., Smith, E. F., Pruss, S. B., Oates, K., Waechter, F., Trotzuk, D., & Fallick, A. E. (2013). The Laurentian record of Neoproterozoic glaciation, tectonism, and eukaryotic evolution in Death Valley, California. *GSA Bulletin*, *125*, 1203–1223. https://doi.org/10.1130/B30789.1

Mahon, R. C., Dehler, C. M., Link, P. K., Karlstrom, K. E., & Gehrels, G. E. (2014). Geochronologic and stratigraphic constraints on the Mesoproterozoic and Neoproterozoic Pahrump Group, Death Valley, California: A record of the assembly, stability, and breakup of Rodinia. *GSA Bulletin*, *126*, 652–664. https://doi.org/10.1130/B30956.1

Martí Mus, M., & Moczydłowska, M. (2000). Internal morphology and taphonomic history of the Neoproterozoic vase-shaped microfossils from the Visingsö Group, Sweden. *Norsk Geologisk Tidsskrift*, *80*, 213–228.

Mitchell, E. A. D., Payne, R., & Lamentowicz, M. (2008). Potential implications of differential preservation of testate amoeba shells for Paleoenvironmental reconstruction in peatlands. *Journal of Paleolimnology*, *40*, 603–618. https://doi.org/10.1007/s10933-007-9185-z

Moczydłowska, M., Pease, V., Willman, S., Wickström, L., & Agić, H. (2017). A Tonian age for the Visingsö Group in Sweden constrained by detrital zircon dating and biochronology: Implications for evolutionary events. *Geological Magazine*, *155*, 1175–1189. https://doi.org/10.1017/S0016756817000085

Morais, L., Fairchild, T. R., Lahr, D. J. G., Rudnitzki, I. D., Schopf, J. W., Garcia, A. K., Kudryavtsev, A. B., & Romero, G. R. (2017). Carbonaceous and siliceous Neoproterozoic vase-shaped microfossils (Urucum Formation, Brazil) and the question of early protistan biomineralization. *Journal of Paleontology*, *91*, 393–406. https://doi.org/10.1017/jpa.2017.16

Ogden, C. G., & Hedley, R. H. (1980). An atlas of freshwater testate amoebae. *Soil Science*, *130*(3), 176. https://doi.org/10.1097/00010694-198009000-00013

Peng, Y., Bao, H., & Yuan, X. (2009). New morphological observations for Paleoproterozoic acritarchs from the Chuanlinggou Formation, North China. *Precambrian Research*, *168*, 223–232. https://doi.org/10.1016/j.precamres.2008.10.005

Porter, S. M., & Knoll, A. H. (2000). Testate amoebae in the Neoproterozoic Era: Evidence from vase-shaped microfossils in the Chuar Group, Grand Canyon. *Paleobiology*, *26*, 360–385. https://doi.org/10.1666/0094-8373(2000)026<0360:TAITNE>2.0.CO;2

Porter, S. M., Meisterfeld, R., & Knoll, A. H. (2003). Vase-shaped microfossils from the Neoproterozoic Chuar Group, Grand Canyon: A classification guided by modern testate amoebae. *Journal of Paleontology*, *77*, 409–429. https://doi.org/10.1666/0022-3360(2003)077<0409:VMFTNC>2.0.CO;2

Porter, S. M., & Riedman, L. A. (2019). Evolution: Ancient fossilized amoebae find their home in the tree. *Current Biology*, *29*, PR212–R215. https://doi.org/10.1016/j.cub.2019.02.003

Preisig, H. R. (1994). Siliceous structures and silicification in flagellated protists. *Protoplasma*, *181*, 29–42. https://doi.org/10.1007/BF01666387

Raven, J. A., & Knoll, A. H. (2010). Non-skeletal biomineralization by eukaryotes: Matters of moment and gravity. *Geomicrobiology Journal*, *27*, 572–584. https://doi.org/10.1080/01490451003702990

Reinhard, C. T., Planavsky, N. J., Gill, B. C., Ozaki, K., Robbins, L. J., Lyons, T. W., Fischer, W. W., Wang, C., Cole, D. B., & Konhauser, K. O. (2017). Evolution of the global phosphorus cycle. *Nature*, *541*, 386–389. https://doi.org/10.1038/nature20772

Riedman, L. A., Porter, S. M., & Calver, C. R. (2018). Vase-shaped microfossil biostratigraphy with new data from Tasmania, Svalbard, Greenland, Sweden and the Yukon. *Precambrian Research*, *319*, 19–36. https://doi.org/10.1016/j.precamres.2017.09.019

Rooney, A. D., Austermann, J., Smith, E. F., Li, Y., Selby, D., Dehler, C. M., Schmitz, M. D., Karlstrom, K. E., & Macdonald, F. A. (2017). Coupled Re-Os and U-Pb geochronology of the Tonian Chuar Group, Grand Canyon. *GSA Bulletin*, *130*, 1085–1098.

Rooney, A. D., Strauss, J. V., Brandon, A. D., & Macdonald, F. A. (2015). A Cryogenian chronology: Two long-lasting synchronous Neoproterozoic glaciations. *Geology*, *43*, 459–462. https://doi.org/10.1130/G36511.1

Smith, E. F., Macdonald, F. A., Crowley, J. L., Hodgin, E. B., & Schrag, D. P. (2015). Tectonostratigraphic evolution of the c. 780–730 Ma Beck Spring Dolomite: Basin Formation in the core of Rodinia. In Z. X. Li, D. D. D. Evans, & J. B. Murphy (Eds.), *Supercontinent cycles through earth history* (Vol. *424*, pp. 213–239). Geological Society of London Special Publications.

Snoeijs, P. J. M., Busse, S., & Potapova, M. (2002). The importance of diatom cell size in community analysis. *Journal of Phycology*, *38*, 265–281.

Strauss, J. V., MacDonald, F. A., Halverson, G. P., Tosca, N. J., Schrag, D. P., & Knoll, A. H. (2015). Stratigraphic evolution of the Neoproterozoic Callison Lake Formation: Linking the break-up of Rodinia to the Islay Carbon isotope excursion. *American Journal of Science*, *315*, 881–944. https://doi.org/10.2475/10.2015.01

Strauss, J. V., Rooney, A. D., Macdonald, F. A., Brandon, A. D., & Knoll, A. H. (2014). 740 Ma vase-shaped microfossils from Yukon, Canada: Implications for Neoproterozoic chronology and biostratigraphy. *Geology*, *42*, 659–662. https://doi.org/10.1130/G35736.1

Wood, R. (2018). Exploring the drivers of early biomineralization. *Emerging Topics in Life Sciences*, *2*(2), 201–212.

Xiao, S., & Knoll, A. H. (1999). Fossil preservation in the Neoproterozoic Doushantuo phosphorite Lagerstätte, South China. *Lethaia*, *32*, 219–240. https://doi.org/10.1111/j.1502-3931.1999.tb00541.x

Young, J. R. et al (2003). A guide to extant coccolithophores taxonomy. *Journal of Nannoplankton Research Special Issue*, *1*, 1–125.

Young, J. R., Geisen, M., & Probert, I. (2005). A review of selected aspects of coccolithophore biology with implications for paleobiodiversity estimation. *Micropaleontology*, *51*, 267–288. https://doi.org/10.2113/gsmicropal.51.4.267

Zlatogursky, V. V. (2013). Puzzle-like cyst wall in centrohelid heliozoans *Raphidiophrys heterophryoidea* and *Raineriophrys erinaceoides*. *Acta Protozoologica*, *52*, 229–236.

Zlatogursky, V. V. (2016). There and back again: Parallel evolution of cell coverings in centrohelid heliozoans. *Protist*, *167*, 51–66. https://doi.org/10.1016/j.protis.2015.12.002

SUPPORTING INFORMATION

Additional supporting information may be found online in the Supporting Information section.

How to cite this article: Riedman LA, Porter SM, Czaja AD. Phosphatic scales in vase-shaped microfossil assemblages from Death Valley, Grand Canyon, Tasmania, and Svalbard. *Geobiology*. 2021;00:1–12. https://doi.org/10.1111/gbi.12439